

Particle bound reactive oxygen species (PB-ROS) emissions and formation pathways in residential wood smoke under different combustion and aging conditions

Jun Zhou¹, Peter Zotter², Emily A. Bruns¹, Giulia Stefenelli¹, Deepika Bhattu¹, Samuel Brown^{1,3}, Amelie Bertrand^{1,4}, Nicolas Marchand⁴, Houssni Lamkaddam¹, Jay G. Slowik¹, André S.H. Prévôt¹, Urs Baltensperger¹, Thomas Nussbaumer², Imad El-Haddad¹, and Josef Dommen¹

¹Laboratory of Atmospheric Chemistry, Paul Scherrer Institute, 5232 Villigen PSI, Switzerland

²Lucerne University of Applied Sciences and Arts, School of Engineering and Architecture, Bioenergy Research, 6048 Horw, Switzerland

³Institute for Atmospheric and Climate Science, ETH, Zurich, Switzerland

⁴Aix Marseille Univ, CNRS, LCE, Marseille, France

Correspondence to: Josef Dommen (josef.dommen@psi.ch)

Abstract. Wood combustion emissions can induce oxidative stress in the human respiratory tract by reactive oxygen species (ROS) in the aerosol particles, which are emitted either directly or formed through oxidation in the atmosphere. To improve our understanding of the particle bound ROS (PB-ROS) generation potential of wood combustion emissions, a suite of smog chamber (SC) and potential aerosol mass (PAM) chamber experiments were conducted under well determined conditions for different combustion devices and technologies, different fuel types, operation methods, combustion regimes, combustion phases and aging conditions. The PB-ROS content as well as the chemical properties of the aerosols were quantified by a novel ROS analyzer using the DCFH (2',7'-dichlorofluorescein) assay and a high resolution time of flight aerosol mass spectrometer (HR-ToF-AMS). For all eight tested combustion devices, primary PB-ROS concentrations substantially increased upon aging. The level of primary and aged PB-ROS emission factors (EF_{ROS}) were dominated by the combustion device (within different combustion technologies) and to a greater extent by the combustion regimes: the variability within one device was much higher than the variability of EF_{ROS} from different devices. Aged EF_{ROS} under bad combustion conditions were ~2-80 times higher than under optimum combustion conditions. EF_{ROS} from automatically operated combustion devices were on average one order of magnitude lower than those from manually operated appliances, which indicates that automatic combustion devices operated at optimum conditions to achieve near-complete combustion should be employed to minimize PB-ROS emissions. The use of an electrostatic precipitator decreased the primary and aged ROS emissions by a factor of ~1.5 which is however still within the burn-to-burn variability. The parameters controlling the PB-ROS formation in secondary organic aerosol were investigated by employing a regression model, including the fractions of the mass to charge ratios m/z 44 and 43 in secondary organic aerosol (SOA) (f_{44-SOA} and f_{43-SOA}), the OH exposure, and the total organic aerosol mass. The regression model results of the

SC and PAM chamber aging experiments indicate that the PB-ROS content in SOA seems to increase with the SOA oxidation state, which initially increases with OH exposure and decreases with the additional partitioning of semi-volatile components with lower PB-ROS content at higher OA concentrations, while further aging seems to result in a decay of PB-ROS. The results and the special data analysis methods deployed in this study could provide a role model for PB-ROS analysis of further wood or any other combustion studies investigating different combustion conditions and aging methods.

1 Introduction

Numerous studies have shown a link between exposure to airborne particulate matter (PM) and worldwide morbidity and mortality (Beelen et al., 2013; Dockery et al., 1993; He et al., 2016), as well as a strong correlation of airborne PM with lung function (Lee et al., 2011; Pope et al., 2002; Adam et al., 2015; Hwang et al., 2015). The adverse health effects of PM are related to the aerosol chemical composition (Kelly and Fussell, 2012; Baltensperger et al., 2008). Residential wood combustion can contribute 5–44 % to the total ambient PM_{2.5} (particulate matter with a diameter smaller than 2.5 µm), depending on the environment (Zhang et al., 2010; EPBE, 2005; USEPA, 2000; EEA, 2013a; Ciarelli et al., 2017). In addition to PM, wood combustion emits a wide range of gaseous pollutants, including volatile organic compounds, which upon oxidation can form secondary organic aerosol (SOA). Although wood is considered to be a climate neutral source of energy, epidemiological studies suggest that wood smoke may contribute significantly to premature mortality (Boman et al., 2003; Johnston et al., 2012), because of its association with respiratory disease, cerebrovascular diseases and impaired lung function (Liu et al., 2017; Yap, 2008; Fullerton et al., 2011). Liu et al. (2017) found a 7.2 % increase in the risk of respiratory hospital admissions during days with high wildfire-specific PM_{2.5} compared to non-wildfire smoke event days. Exposure to wood combustion particles may cause moderate inflammatory activity, cell death and DNA damage, and adverse effects to airway epithelia (Krapf et al., 2017; Tapanainen et al., 2012; Muala et al., 2015; Marabini et al., 2017). These adverse effects may be related to oxidative stress caused by free radicals induced by inhaled PM, which overwhelms the antioxidants in the body (Lobo et al., 2010).

This may happen via two pathways. 1) Particles may contain reactive oxygen species (particle-bound ROS, PB-ROS, exogenous), which act as oxidants in the biological system; 2) particles may contain transition metals or organic compounds like quinones, which generate reactive oxygen species by interaction with physiological species undergoing Fenton reactions and redox cycling. For the measurement of the latter property several assays have been introduced, where the loss of reductants like dithiothreitol (DTT), glutathione (GSH) or ascorbic acid (AA) is measured (Cho et al., 2005; Verma et al., 2012; Charrier and Anastasio, 2012; Verma et al., 2015; Fang et al., 2016; Weber et al., 2018; Mudway et al., 2004; Li et al., 2003; Fang et al., 2016). Also cellular tests with an ROS probe have been developed to measure ROS induced by aerosols in a biotic system (Landreman et al., 2008; Zhang et al., 2016; Tuet et al., 2017). The DCFH assay has been shown to be sensitive to a broad range of organic peroxides, alkyl peroxide radicals, and hypochlorite, but not to components that are known to induce redox cycling (i.e., metal ions and quinones) (Venkatachari and Hopke, 2008; Wang et al., 2011; King and Weber, 2013; Fuller et al., 2014b; Zhou et al., 2018). The DCFH assay has fast response rates and a linear response to varying ROS concentrations, for

which reason it was applied as a suitable measure for the PB-ROS concentration (Zhou et al., 1997; Venkatachari and Hopke, 2008; King and Weber, 2013, Zhou et al., 2018).

Several studies tried to establish links between such measurements and specific inflammatory biomarkers of oxidative stress in cell cultures or human subjects. For example Delfino et al. (2010; 2013) found that macrophage ROS generation from PM_{2.5} was significantly positively associated with nitric oxide exhaled from elderly subjects and school children with persistent asthma. Janssen et al. (2015) reported a significant association between exhaled nitric oxide and increases in interleukin-6 in nasal lavage and the ROS generation measured by DTT and AA. Others found correlations between DTT activity and emergency department visits for asthma/wheezing and congestive heart failure (Bates et al., 2015; Fang et al., 2016). We are not aware of a study that relates measurements of ambient PB-ROS by DCFH with inflammatory biomarkers. However, it was shown that fresh SOA can release OH and H₂O₂ when dissolved in water (Wang et al., 2011; Tong et al. 2016). This phenomenon was attributed to labile peroxides contained in SOA, which were shown to decay with a rather short lifetime of less than an hour (Krapf et al., 2016). Lakey et al. (2016) modeled the ROS produced in the human respiratory tract upon inhalation of PM and showed that the OH production rate from SOA can be as high as the H₂O₂ production rate from trace metals. This indicates that PB-ROS might also lead to oxidative stress. Obviously, further research is needed to establish a link between PB-ROS and health effects.

Based on these considerations we performed a study with a DCFH assay to focus on exogenous PB-ROS formed by wood combustion exhaust and during its atmospheric aging. For this purpose, a suite of SC and PAM experiments were conducted. As different types of wood, combustion appliances and combustion conditions result in varying levels of emissions (Johansson et al., 2004; Schmidl et al., 2011; Fitzpatrick et al., 2007; Heringa et al, 2011), eight wood combustion devices with variable combustion conditions were tested. Primary and aged biomass smoke generated under different combustion and aging conditions were characterized by an online ROS analyzer based on the DCFH assay coupled with an aerosol collector. Observations from this study provide more detailed evidence of the influence of combustion technology on the PB-ROS of the emitted PM compared to a previous similar study (Miljevic et al., 2010). We also show the variation of the PB-ROS content from primary and aged aerosols under different operation conditions. Further, the contribution of reactive oxygen species to aged organic aerosol generated with different aging tools was investigated to clarify the PB-ROS formation potential upon photo-oxidation. Results from these experiments may be directly compared with ambient measurements.

2 Experimental setup and methodology

We performed two sets of measurement campaigns, utilizing several wood combustion devices with different combustion conditions and two aging tools. First we present the different devices, then give a description of the PAM chamber and the Paul Scherrer Institute (PSI) mobile smog chamber (PSI-MSM, ~ 7 m³) and the PSI stationary smog chamber (PSI-SSC, 27 m³) (Platt et al., 2013, 2014; Paulsen et al., 2005), including the experimental procedures, and finally discuss the combustion conditions and measurement strategy. An experiment schematic is shown in Figure S1. The combustion devices, experiment aging tools, as well as the test aspects are listed in Table 1.

2.1 Combustion devices

Eight combustion devices with different technologies were tested, including a pellet boiler (PB, automatic), a moving grate boiler equipped with electrostatic precipitator (MGB, automatic), a updraft combustion pellet stove (PS, automatic), a two-stage combustion downdraft log wood boiler (LWB, manual), two advanced two-stage combustion log wood stoves (LWS1, manual, updraft; LWS2, manual, updraft combustion when cold and downdraft combustion when hot), and two conventional single-stage combustion log wood stoves (LWS3: manual, and LWS4: manual). In the following, we describe the different combustion devices.

PB. Automatically operated pellet boiler, with two-stage updraft combustion and a nominal heat output of 15 kW, using wood pellets (EN certified, moisture content 7 %) as the combustion fuel. Under optimum combustion conditions, the ideal air to fuel ratio (λ) is achieved leading to near-complete combustion and, consequently, the particle emissions are dominated by inorganic components which are contained in the pellets. The PB was also altered to enable the variation of the air to fuel ratio to investigate the influence of this parameter on the emissions. In this way, different combustion regimes could be achieved with this device, details are described in Sect. 2.2.

MGB. Automatically operated industrial moving grate boiler with nominal heat output of 150 kW, operated with wood chips (30 % moisture content). The grate has several zones where primary and secondary combustion air can be regulated.

PS, LWB, LWS1, LWS2, LWS3 and LWS4. LWB, LWS1 and LWS2 are advanced stoves/boilers with two-stage combustion technology, while in LWS3 and LWS4 conventional single-stage updraft combustion is applied. PS is an automatically operated pellet stove with a nominal heat output of 6 kW under full load. It possesses a ventilator for the injection of the combustion air. However, due to a relatively simple air control, the PS is operated at high λ . We also investigated part load conditions at 3 kW. LWB, LWS1, LWS2, LWS3 and LWS4 are manually operated devices, with the nominal heat outputs of 30 kW, 8 kW, 4.6 kW, 8 kW and 4.5 kW, respectively. Further, the LWS1 is equipped with a storage container for logs, which slide on the grate due to gravity. For all four two-stage combustion devices (PS, LWB, LWS1, and LWS2) and one single-stage combustion device (LWS3), PB-ROS emissions from starting, flaming and burn out phases were investigated (details of the combustion phases are described in Sect. 2.3). In the case of the LWS4, only the flue gas from the flaming phase was injected into the smog chamber, where the EF_{ROS} under different aging temperatures of -10 °C and 15 °C were tested. In three of the log wood operated devices (LWS1, LWS2 and LWS3) dry (13–16 % moisture content) and wet logs (24–42 % moisture content) were investigated. In the PS, wheat pellets (manufactured from milling residues, moisture content 9 %) were tested in addition to conventional wood pellets (EN certified, moisture content of 7 %). In the LWS4, beech wood logs with a moisture content of 18 ± 3 % were used.

2.2 Combustion conditions

140 Two parameters are used to describe the combustion conditions namely the combustion regimes and the combustion phases. Combustion regimes are defined by the air fuel equivalence ratio (λ) (Nussbaumer et al., 2000).

$$\lambda = \frac{O_{2,amb}[\%]}{O_{2,amb}[\%] - O_{2,flue\ gas}[\%]} \quad (1)$$

where $O_{2,amb}$ and $O_{2,flue\ gas}$ are the oxygen contents in ambient air ($O_{2,amb} = 21$) and in the flue gas, respectively. Depending mainly on the level of excess air three combustion regimes are distinguished: lack of oxygen (λ^-),
145 optimum combustion condition (λ^{opt}), and (high) excess of oxygen (λ^{++}). Each of these is characterized by a different type of combustion particles, i.e., comprising mostly soot, salts, and condensable organic compounds, respectively (Nussbaumer and Lauber, 2010). It should be noted that in wood combustion λ is always > 1 . Consequently, λ^- and λ^{++} only describe λ -values which are clearly (for λ^{++} at least 1.5 fold or higher) below or above λ^{opt} .

150 The three combustion regimes were achieved by changing the air to fuel ratio in the pellet boiler (PB). Optimum combustion conditions (λ^{opt}) were easily achieved by operating the PB under the designed optimum operation mode. High excess of oxygen (λ^{++}) compared to λ^{opt} was obtained by additionally blowing air into the combustion chamber via the ignition tube. The lack of oxygen (λ^-) regime was obtained by manually closing the secondary combustion air inlet. It should be noted that in real life operation λ^{++} and λ^- conditions only occur with severe mal-operation. These
155 conditions were investigated since they result in distinct emission characteristics (high NMVOC emissions during λ^{++} and high soot emissions during λ^- (Nussbaumer and Lauber, 2010).

In the MGB, part load (50 kW) and full load (150 kW) conditions were tested, as well as the influence of an electrostatic precipitator (ESP) installed downstream of the combustion unit. ESPs are widely used in both large and small scale wood combustion devices to reduce PM emissions (Bologa et al., 2011; Nussbaumer and Lauber, 2010).

160 Combustion phases in the log wood stoves, log wood boiler and pellet stove were classified using the modified combustion efficiency (MCE), defined as the molar ratio of the emitted CO_2 divided by CO plus CO_2 ($CO_2/(CO+CO_2)$), in the flue gas after wood combustion (Ward and Radke, 1993). Each full combustion cycle includes three combustion phases: start phase (beginning of the burning cycle before MCE reaches 0.974), flaming phase (between start and burnout phase, with $MCE > 0.974$) and burnout phase (after flaming phase, with $MCE <$
165 0.974). As mentioned in Sect. 2.1, all three phases were obtained in the PS, LWB, LWS1, LWS2 and LWS3. In the PS, LWB and LWS1, experiments started with a cold start, followed by a flaming phase and burn out. In the LWS2 and LWS3, after the first complete combustion cycle starting with a cold start, several full combustion cycles followed by adding new logs into the combustion chamber after the burn out was finished (warm start). In devices where the combustion phases were rapidly changing the ROS analyzer was not able to separate these combustion
170 phases due to a slow response time (~ 8 min). Consequently, the single combustion phases, including the start, flaming and burn out, as well as the combined combustion phases start + flaming or flaming + burn out were used

for the PB-ROS analysis. In the LWS4, with which the experiments were conducted in the PSI-MSC (at temperatures of 263 K and 288 K), and the PSI-SSC (at a temperature of 288 K), only emissions from the flaming phase were sampled.

2.3 Experimental procedures and aging tools

2.3.1 PAM chamber

Seven combustion devices (except LWS 4) were tested using the PAM chamber as an aging tool. The emissions were sampled through a heated line (473 K), diluted by a factor of ~100-150 using two ejector diluters in series (VKL 10, Palas GmbH), and then injected into the PAM chamber (see Figure S1 in the Supporting Information).

The original concept of the PAM chamber is described by (Kang et al., 2007). Briefly, the PAM chamber is a single, 0.015 m³ cylindrical glass chamber, flanked by two UV lamps. Prior to entering the PAM chamber, pure air (1.6 L min⁻¹, humidified with a Nafion membrane, Perma Pure LLC) used as an OH precursor and a stream of diluted d9-butanol (98%, Cambridge Isotope Laboratories) were merged with the incoming reactant flow. The OH exposure during aging was defined as the integral of the OH concentration over the reaction time, and was calculated from the decay of the d9-butanol, measured by a proton transfer reaction–mass spectrometer (PTR-MS 8000, Ionicon Analytik GmbH) (Barnett et al., 2012). The total flow rate in the PAM chamber was maintained at ~ 7 L min⁻¹, which was the sum of the flow rates of the instruments and a supplementary flow, resulting in a residence time of approximately 2 minutes. The OH exposure was controlled by adjusting the UV light intensity to obtain different OH concentrations. An outer ring flow (~0.7 L min⁻¹), which was discarded, was used to minimize wall losses and the instrument sampled only from the inner flow of the PAM chamber (~6.3 L min⁻¹). The temperature in the PAM chamber was around 38 °C due to the lamps. Primary wood combustion emissions were characterized either before or after the PAM chamber when the lights were switched off. Aged emissions were characterized after the PAM chamber with lights on. All the experiments were conducted under OH exposures of (1.1-2.0)×10⁸ molec cm⁻³ h which corresponds to ~ 4.5-8 days of aging in ambient by assuming a mean daily OH concentration of 1×10⁶ molec cm⁻³. The applicability of the PAM chamber to measure wood combustion emissions has been shown in a previous study (Bruns et al., 2015).

2.3.2 Smog chamber aging

The second set of experiments was conducted in the PSI mobile smog chamber (PSI-MSC, ~ 7 m³) at temperatures of 263 K and 288 K, and the PSI stationary smog chamber (PSI-SSC, 27 m³) at 295.5 K. An overview of the experimental setup is also shown in Figure S1. Generally, 3 pieces of dry beech logs, 4 pieces of kindling and 3 fire starters and 9 pieces dry beech logs, 8 pieces kindling and 4 fire starters were combusted in LWS4 for average (2.9 ± 0.3 kg) and high (5.1 kg) load experiments, respectively (details in Sect. 2.1). The wood moisture content was 19 ± 2 %. Only emissions during the flaming phase with a modified combustion efficiency (MCEs) in the range from 0.974 to 0.978 were sampled. Emissions were sampled for 11-21 min and injected into the PSI-MSC using an ejection diluter, yielding a total dilution factor of 100 to 200. Hydroxyl radical (OH) concentrations in the chamber are controlled by continuous injection of nitrous acid into the smog chamber (after the characterization of the primary

emissions as described below in Sect. 3.1), which produces OH upon irradiation by UV lights (Platt et al., 2013). The OH exposure was estimated by monitoring the decay of d9-butanol (butanol-D9, 98%, Cambridge Isotope Laboratories) following a single injection before the UV lights were turned on. In all five experiments conducted in the PSI-MSC, the aging time lasted 4.5-6 h. The OH exposure was $2.6-4.8 \times 10^7$ molec cm⁻³ h which corresponds to ~1-2 days of aging in ambient by assuming a mean daily OH concentration of 1×10^6 molec cm⁻³. More details about some of the PSI-MSC experiments of this campaign can also be found in Bruns et al. (2016, 2017). One additional experiment was conducted in the PSI-SSC, with an OH exposure up to 4.0×10^8 molec cm⁻³ h, equivalent to ~17 days of aging assuming a mean daily OH concentration of 1×10^6 molec cm⁻³, extending the aging range beyond the range achieved by the PAM chamber (~1-8.5 days).

2.4 Particle phase characterization

The non-refractory particle chemical composition was measured using a high resolution time-of-flight aerosol mass spectrometer (HR-ToF-AMS, flow rate: 0.1 L min⁻¹, Aerodyne Research Inc.) (DeCarlo et al., 2006). The HR-ToF-AMS measured the total organic aerosol (OA), SO₄²⁻, NO₃⁻, NH₄⁺, Cl⁻, as well as the two most dominant oxygen-containing ions in the OA spectra, i.e., the mass to charge ratios m/z 44 (Org44, mostly CO₂⁺) and m/z 43 (Org43, mainly C₂H₃O⁺ for the oxygenated OA and C₃H₇⁺ for the hydrocarbon-like OA) (Ng et al., 2011). Equivalent black carbon (eBC) was determined using an Aethalometer (AE33, Magee Scientific; flow rate: 2 L min⁻¹, Drinovec et al., 2015).

The particle bound ROS was characterized by an on-line ROS analyzer (flow rate: 1.7 L min⁻¹) (Zhou et al., 2018). The aerosols particles were collected in a mist chamber type aerosol collector, dissolved into water and mixed with a 2',7'-dichlorofluorescein (DCFH)/horseradish peroxidase solution. The ROS converts DCFH to DCF, which is detected by fluorescence and quantified as nM-H₂O₂ equivalents. The time resolution of the on-line ROS analyzer was ~ 8 minutes, preventing resolving brief discrete combustion phases. Therefore, different methods were used to calculate the average PB-ROS emissions under different conditions:

- 1) average (Figure S2a): utilized when the combustion conditions were relatively stable and sufficiently long to yield a stable ROS signal;
- 2) integrated average (Figure S2b): in cases of variable combustion conditions, the ROS signal was integrated over the measurement period which could include one or several phases from the same burn;
- 3) extrapolation + integrated average (Figure S2: panels 2c_1 and c_2): when the combustion conditions were variable and the background could not be measured between two combustion conditions due to the time resolution of the ROS instrument. We extrapolate each measurement to the background value and then make the integrated average calculation as described above.

The various definitions for PB-ROS and related aerosol characteristics are presented below:

PB-ROS emission factors (EF_{ROS}). PB-ROS emission factors (EF_{ROS}) were calculated as the amount of PB-ROS in nmol-H₂O₂ equivalents per kilogram wood burnt, using Eq. (2):

$$EF_{ROS} = \frac{n_{ROS}}{M_c} C_{wood} \cong \frac{[n_{ROS}]}{\Sigma([\rho C_{CO_2}] + [\rho C_{CO}] + [\rho C_{CH_4}] + [\rho C_{VOC}] + [\rho C_{eBC}] + [\rho C_{OC}])} C_{wood} \quad (2)$$

where $[n_{ROS}]$ is the background-corrected concentration of PB-ROS (nmol m^{-3}) in the emitted particles either before (primary PB-ROS) or after aging (aged PB-ROS), $[\rho C_x]$ are the carbon mass concentrations calculated from the background-corrected, carbon-containing species where x includes CO_2 , CO , CH_4 , volatile organic compounds (VOC), eBC, and particulate organic carbon (OC). M_c is the carbon mass burnt and C_{wood} represents the average carbon fraction of the wood fuel, ~ 0.46 , measured in this study using an elemental analyzer. OC data were obtained from AMS measurements. Similarly, the organic aerosol (OA) emission factors (EF_{OA}) were calculated by replacing the PB-ROS concentration by OA.

PB-ROS fraction. In order to study the PB-ROS formation during aging, the secondary PB-ROS fraction ($f_{ROS-SOA}$) is introduced. It expresses the amount of secondary PB-ROS ($ROS_s = \text{aged ROS} - \text{primary ROS}$) per amount of secondary organic aerosol (SOA) formed during aging and as calculated from Eq. (3)

$$f_{ROS-SOA} = \frac{ROS_s}{SOA} \quad (3)$$

Secondary organic aerosol (SOA) and secondary PB-ROS (ROS_s) were calculated by subtracting primary organic aerosol (POA) and primary PB-ROS (ROS_p) from the total OA and aged PB-ROS, respectively, assuming ROS_p and POA to be only lost to the chamber wall at the same rate as eBC but otherwise to remain constant during aging. Although both quantities may not be conserved, a decrease of both does partially compensate in the PB-ROS fraction. In the SC experiments, POA is defined as the OA mass before lights on, while SOA is estimated as the difference between total OA and the time dependant POA mass accounting for particle wall loss. Wall loss rates for POA and SOA were assumed to be the same as that of the measured eBC. In PAM aging experiments, each experiment had a certain POA (measurements before PAM or after PAM with lights off) and SOA (measurements after PAM with lights on).

f_{44-SOA} and f_{43-SOA} . To express the degree of oxygenation of SOA, the fraction of secondary Org44 and Org43 in SOA (represented as f_{44-SOA} and f_{43-SOA}) is introduced, which is calculated from Eq. (4)

$$f_{44-SOA} = \frac{Org_{44-SOA}}{SOA}; f_{43-SOA} = \frac{Org_{43-SOA}}{SOA} \quad (4)$$

where Org_{44-SOA} is the difference of total Org44 and primary Org44, Org_{43-SOA} is the difference of total Org43 and primary Org43 and using the same procedure as for the SOA calculation mentioned above.

Wall loss correction. The wall loss correction in the SC was done by assuming the same losses for all particle components as for the inert tracer eBC. The wall loss corrected concentration of OA or PB-ROS (X) can be derived using the equation Eq. (5):

$$X_{WLC}(t) = X_{meas}(t) \times \frac{BC(t_0)}{BC(t)} \quad (5)$$

where $X_{meas}(t)$ refers to the concentration of X measured at time t . $BC(t_0)$ and $BC(t)$ are the concentrations of BC when lights were switched on and at time t , respectively.

2.5 Gas phase characterization

During the PAM chamber experiments, total volatile organic compounds (VOC) and CH_4 (using a flame ionization detector (FID) with a non-methane cutter, model 109A, J.U.M Engineering), CO and NO (with a non-dispersive infrared analyzer, Ultramat 23 Siemens) as well as O_2 (using a paramagnetic oxygen analyzer, Ultramat 23 Siemens) were determined in the hot undiluted flue gas. In SC aging experiments CO was measured with a cavity ring-down spectrometer (G2401, Picarro, Inc.). In all experiments, the composition of VOCs was determined by a proton transfer reaction–mass spectrometry (PTR-MS 8000, Ionicon Analytik GmbH). For CO_2 a cavity ring-down spectrometer (G2401, Picarro, Inc.) was used in the SC aging experiments and a non-dispersive infrared (NDIR) analyzer (model LI-820, LI-COR®) in the PAM chamber aging experiments.

3 Results and discussion

3.1 Primary and aged PB-ROS emission factors (EF_{ROS})

The PB-ROS and OA emission factors are presented in Table 2 for all combustion condition, together with the number of tests, the combustion efficiency (MCE), the air to fuel ratio (λ), and the aerosol bulk properties determined with the AMS (OM:OC, O:C and H:C ratios). The given values are the 25 percentile and 75 percentile of averages from several experiments and the data points considered for the calculations were restricted to the time period of the PB-ROS measurements. As shown in Fig. 1, PB-ROS emission factors (EF_{ROS}) for primary and aged OA were highly variable depending on the combustion conditions and devices. For all devices and combustion conditions, a substantial enhancement in the EF_{ROS} is observed with aging, indicating the importance of secondary PB-ROS production. The PB-ROS enhancement factor, defined as the ratio between aged and primary EF_{ROS} , range between 4 and 20, with lower values for MGB (~ 4) and PB under λ^{opt} combustion condition (~ 6), and higher values for PB under λ^- and λ^{++} combustion conditions (> 10). The PB-ROS enhancement factors for all log wood stoves as well as LWB are comparable, with an average value around 10.

The variability in the EF_{ROS} in primary and aged OA for one device is much higher than the variability between average emission factors for different devices, spanning almost two orders of magnitudes. Despite this, EF_{ROS} from PB and MGB (80-8 890 nmol kg⁻¹ wood and 2 440-1.83×10⁵ nmol kg⁻¹ wood for primary and aged emissions, respectively) are on average one order of magnitude lower than those from PS, LWB and LWS1-4 (220-1.89 × 10⁶ nmol kg⁻¹ wood and 3 570-1.1×10⁶ nmol kg⁻¹ wood for primary and aged emissions, respectively). These results clearly indicate differences due to the combustion technology, as a general rule, EF_{ROS} were lowest for automatically operated devices and higher for manually operated devices: PB and MGB are automatically operated and the primary and secondary air supply as well as the fuel feeding is controlled permanently, while LWB and LWS1-4 are manually operated. The PS is automatically operated but is operated at high λ and exhibits similar EF_{ROS} to the

manual devices. Part of the EF_{ROS} variability within each device can be ascribed to the combustion phase, with higher emission factors for the starting and burn out phases compared to the flaming/stable phase. This is especially true for the aged emissions from the PS (EF_{ROS} of the start phases was on average 13 times higher than the flaming phase; Mann-Whitney p -value = 0.06), the LWS2 (EF_{ROS} of the start phases was on average 1.7 times higher than the flaming phase, Mann-Whitney p -value = 0.24, not significant) and the LWS3 (EF_{ROS} of the start and burn out phases were on average 1.5 times higher than the flaming and flaming + burn out phase, Mann-Whitney p -value = 0.07).

For the automatically operated MGB, the primary EF_{ROS} did not statistically differ between part and full load operation (Mann-Whitney p -value = 0.95). However, the aged EF_{ROS} was a factor of ~ 3 higher for part load than for full load (Mann-Whitney, p -value = 0.23). The use of the electrostatic precipitator decreased primary and aged ROS emissions, on average by a factor of ~ 1.5 times, however, these differences are not statistically significant (Mann-Whitney p -value = 0.12 for both primary and aged emissions) and are within the burn-to-burn variability.

For PB, the combustion operation could be systematically varied to investigate the influence of air to fuel ratio on PB-ROS and OA emission factors before and after aging. The EF_{ROS} were highest under λ^{++} condition for both primary and aged emissions, with average values of $4\ 100$ and 5.8×10^4 nmol kg⁻¹ wood burnt, respectively (Fig. 1 and Table 2). Primary PB-ROS emissions under λ^{opt} conditions did not statistically differ from λ^- conditions (Mann-Whitney, p -value = 0.43), but on average 7 and 3 times lower than that obtained under λ^{++} condition, respectively (Mann-Whitney, p -value < 0.005 for both cases). The aged EF_{ROS} under λ^{opt} and λ^- were also quite similar (Mann-Whitney, p -value = 0.20), but with average values 8 and 5.5 times lower than obtained under λ^{++} conditions, respectively (Mann-Whitney, p -value = 0.02 for both cases). This shows that the air to fuel ratio has a significant effect on the PB-ROS emissions, which will be investigated for all devices hereafter.

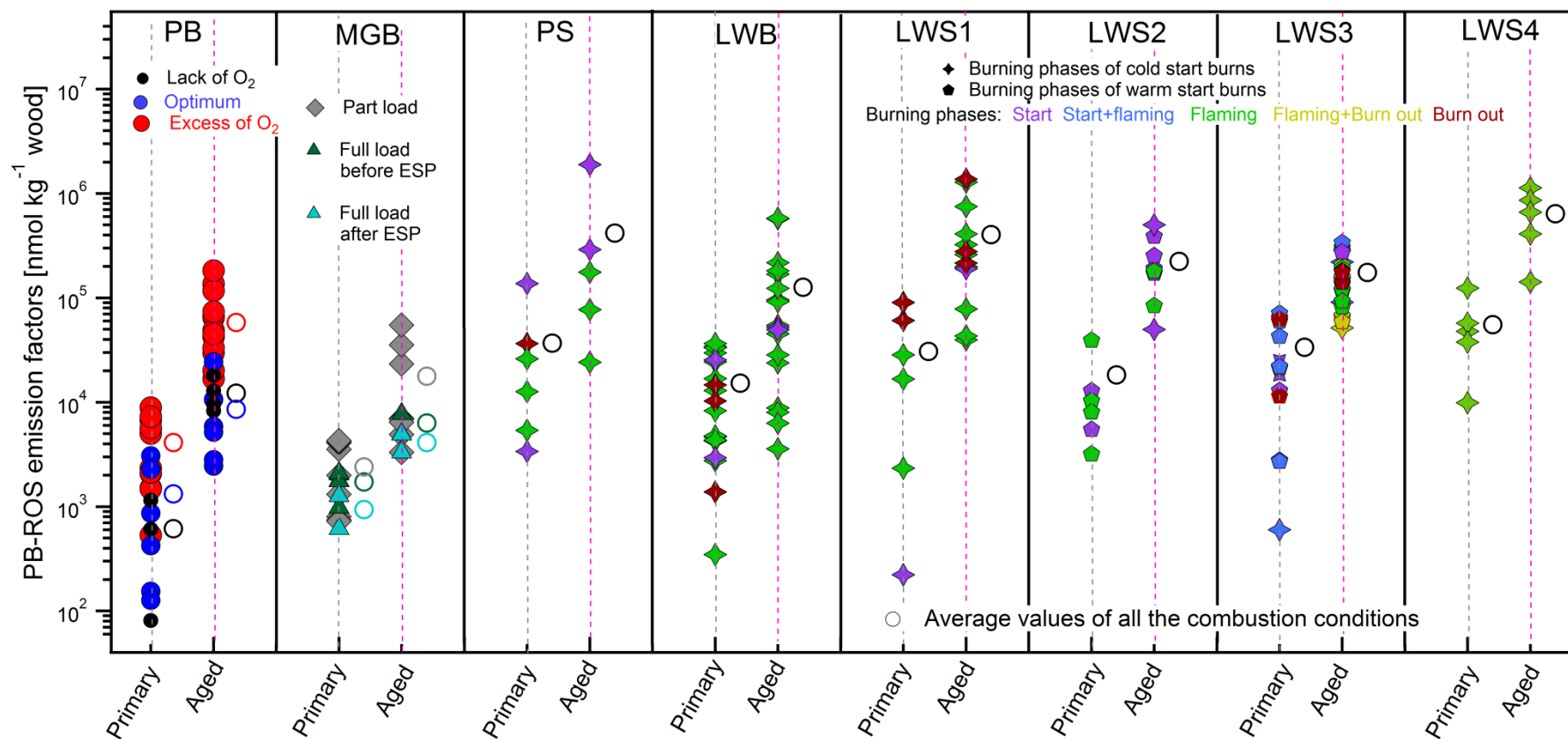


Figure 1. PB-ROS emission factors (EF_{ROS}) for all tested combustion devices under different operating and aging conditions. Open circles symbols represent the average values of all the experimental data points for each condition. PB denotes Pellet boiler; MGB Moving grate boiler; PS Pellet stove; LWB Log wood boiler; LWS n Log wood stove n ($n = 1, 2, 3, 4$). Each data point represents one experiment. For each device, primary EF_{ROS} appear on the left side (gray dashed line) and aged EF_{ROS} on the right side (pink dashed line)

3.2 Aged EF_{ROS} under different combustion regimes

Fig. 2 shows the aged EF_{ROS} of the eight devices as a function of λ . Similar to PB, as already described above, a clear increase of EF_{ROS} in the aged aerosol can be observed with increasing λ values, with ~2-80 times higher aged EF_{ROS} values under bad combustion conditions than under optimum combustion conditions, although the extend of the increase and the overall trend were not the same for all individual devices. In the MGB all the burns occurred at $2.0 < \lambda < 2.2$, leading to aged EF_{ROS} (without ESP) in line with those from the PB between λ^{opt} ($\lambda = 1.6$) and λ^{++} (λ ranged from 2.7-3.4). The combustion in all stoves (PS, LWS1-4) exhibited higher λ ($\lambda > 2.2$) due to a less controlled air supply leading to less efficient combustion. In this excess of oxygen range, aged EF_{ROS} ranged between 1.68×10^4 nmol kg⁻¹ wood and 1.38×10^6 nmol kg⁻¹ for λ values between 2.2-17.6, where all aged EF_{ROS} were high but without any systematic trend with λ , suggesting that other parameters may influence PB-ROS emissions as well. The LWB follows a different trend, where the aged EF_{ROS} increase sharply with λ , starting at lower λ values than the other manually operated devices. Aged EF_{ROS} for LWB ranged from 3530 to 5.79×10^5 nmol kg⁻¹ wood within the λ -range of 1.5-2.6. Although trends in Fig. 2 show differences between devices, they highlight quite readily the important influence of the combustion conditions on aged EF_{ROS} .

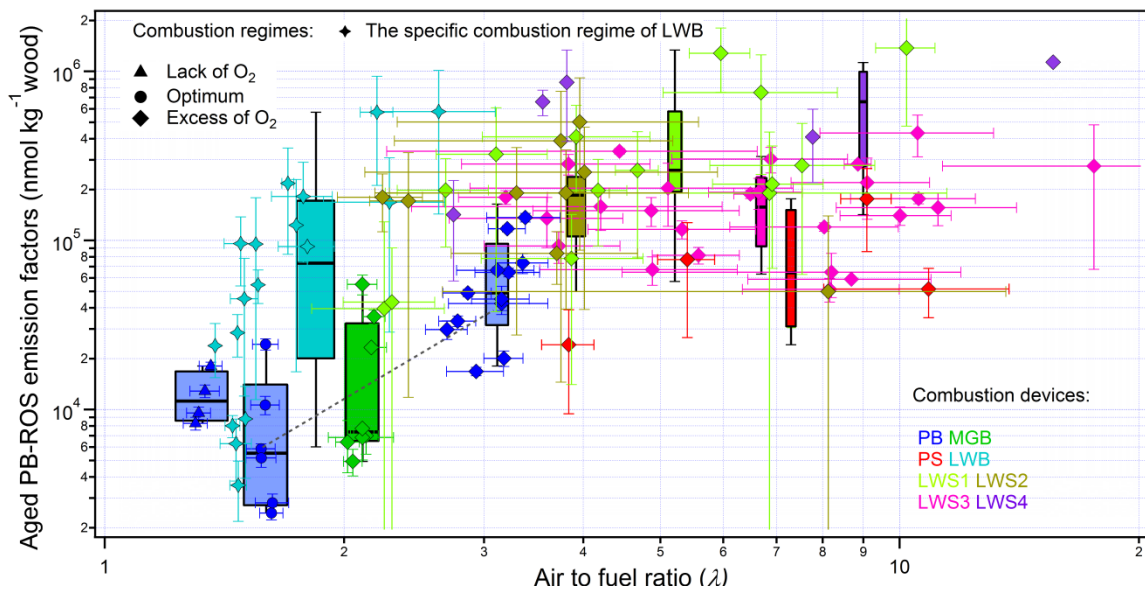


Figure 2. Aged PB-ROS emission factors (EF_{ROS}) from different combustion regimes and combustion devices. The grey dashed line represents the EF_{ROS} increase with λ for the PB. The error bars of the y-axis of the data points denote the propagation of the uncertainty ($\delta = \sqrt{\delta_1^2 + \delta_2^2}$, with δ_1 and δ_2 representing the standard deviation of the averaged aged PB-ROS and aged OA of the measurement time periods, respectively.); the error bars of the x-axis of the data points denote the standard deviation of the averaged λ of the measurement time periods.

While the combustion efficiency was found to have a strong influence on aged EF_{ROS} , the latter varies considerably, by a factor of 3-50, within the same combustion regime but for different combustion devices. In Fig. 3, we investigate to which extent this variability in aged EF_{ROS} is related to the variability in the bulk OA emissions. The high correlation (Pearson's $R = 0.92$) observed in Fig. 3 suggests that changes in aged EF_{OA} explain a great fraction of the variability in aged EF_{ROS} , implying that this variation is inherent to wood combustion conditions. Nonetheless, additional unexplained variation was observed between the two variables

in Fig. 3, with the aged PB-ROS emission factors varying by a factor of 2.6 on average for the same aged EF_{OA} . To elucidate the reasons behind this variability, we investigate in the following the parameters controlling the secondary PB-ROS formation and its content in OA upon aging.

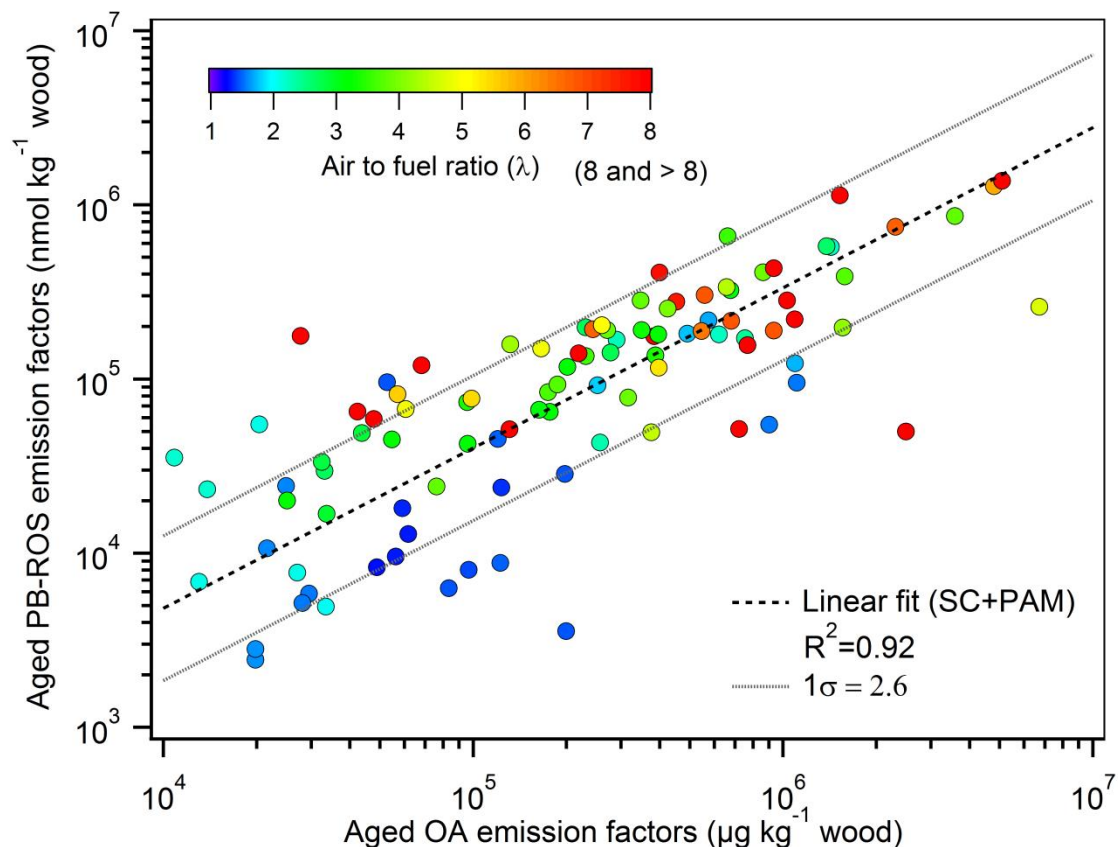


Figure 3. Aged PB-ROS emission factors vs. aged OA emission factors. Marker color correspond to the air to fuel ratio (λ). Fitting equation: $\log_{10}(EF_{ROS}) = 0.92\log_{10}(EF_{OA})$ indicating that the relationship between aged PB-ROS and aged OA is almost linear. The geometric standard deviation obtained from the fit is 2.6, suggesting that the aged PB-ROS content of aged OA may vary significantly depending on the combustion and atmospheric aging conditions.

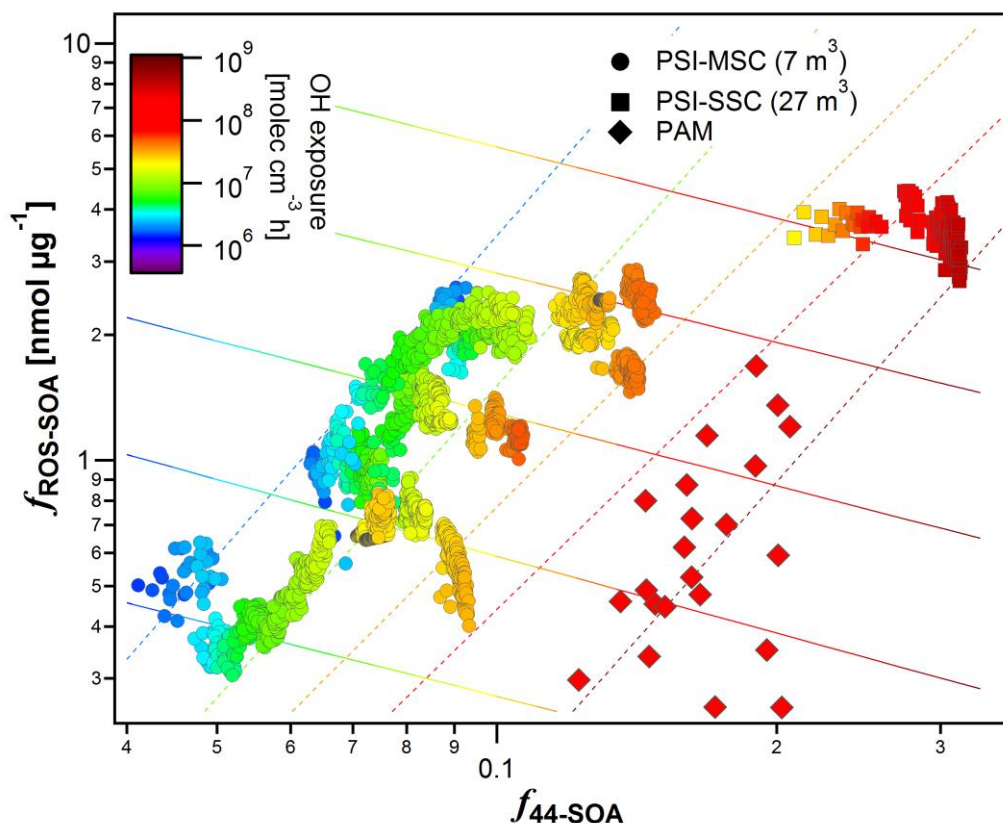


Figure 4: Variation of the fraction of PB-ROS in SOA, $f_{ROS-SOA}$, with the fraction of m/z 44 in the total signal SOA as measured by the AMS (f_{44-SOA}) color coded with the OH exposure estimated from the decay of d9-butanol measured by the PTR-ToF-MS. Data are collected from two different smog chambers (SC) and from the PAM chamber. Dashed lines are isopleths of constant OH exposures, while solid lines are obtained by isolating the effect of OH exposure from other variables. To help discerning different experiments performed in SC, the same content in this figure is plotted again in Fig. S3, where those SC experiments are labeled by different numbers.

Regression model setup and performance. In this section, we seek to evaluate the relationship between the fraction of PB-ROS in SOA, $f_{ROS-SOA}$, and parameters controlling its formation. To exclude the influence of the combustion devices, the data obtained using the LWS4 in the SC experiments and using the LWS3 in the PAM chamber experiments was chosen for the analysis, as the LWS3 and LWS4 are both conventional single-stage combustion devices. Four different parameters were investigated, including f_{43-SOA} and f_{44-SOA} , the OH exposure, and the organic aerosol mass, by running the regression model as follows:

$$f_{ROS-SOA} = a \times SOA + b \times f_{44-SOA} + c \times f_{43-SOA} + d \times (OH \text{ exposure}) + intercept \quad (6)$$

f_{43-SOA} and f_{44-SOA} are believed to represent the contributions of moderately oxygenated components (e.g. alcohols and carbonyls) and highly oxygenated components (e.g. carboxylic acids and peroxides), respectively. The organic aerosol mass may influence the fraction of PB-ROS in SOA, by affecting the amount of condensing semi-volatile species, which might be characterized by different $f_{ROS-SOA}$ compared to low-volatility species dominating at low organic aerosol mass. The aim of the multiple regression analysis used here is to extract the influence of different aging factors on the observed variance in $f_{ROS-SOA}$ (the 2.6 factor variance described in Fig.

3), and to assess the magnitude of their influence. We do, however, not seek to propose using the model and the model coefficients for a deterministic explanation of PB-ROS formation.

Since the dependent variable, $f_{\text{ROS-SOA}}$, and the predictors considered are lognormally distributed – typical of concentrations and contributions –, we have log-transformed the data before the multiple regression analysis.

We note though that this step did not influence the conclusions of the analysis, as a multi-linear model applied to the raw data without a prior log-transformation suggests a similar relationship between $f_{\text{ROS-SOA}}$ and the predictors. Both models reasonably represented the measurements ($\sim 20\%$ error, Fig. S4), but log-transforming the data allowed for a better capturing of lower $f_{\text{ROS-SOA}}$ and a less skewed distribution of the model residuals (Fig. S4). We did not consider any interactions between the different regressors, as this is taken into account through the prior log-transformation of the data. For the parameterization, we only considered the SC data and will discuss whether the PAM chamber data could be satisfactorily explained by the same parameterization or whether the amount of PB-ROS formed under different conditions, with high OH concentrations in the PAM chamber, is different.

We note that the different predictors exhibit some degree of collinearity. For example, not unexpectedly, $f_{44\text{-SOA}}$ significantly increases with aging (R^2 between $f_{44\text{-SOA}}$ and OH exposure = 0.68), while $f_{43\text{-SOA}}$ increases with the amount of organic aerosol in the smog chamber ($R^2 = 0.56$), possibly due to the enhanced partitioning of the moderately oxidized organic species at higher absorptive mass (Pfaffenberger et al., 2013). Both variables, $f_{44\text{-SOA}}$ and $f_{43\text{-SOA}}$, are slightly inversely correlated ($R^2 = 0.26$). Therefore, prior to the regression analysis we inspected the severity of multicollinearity by computing the variance inflation factors (VIF) for all four predictors. All VIF values were between 2.5 and 6 (highest for $f_{44\text{-SOA}}$ and for OH exposure), indicating a moderate degree of multicollinearity (VIF values above 10 would be related to excessive multicollinearity). While a direct consequence of multicollinearity is an increased probability of erroneously rejecting the dependence of $f_{\text{ROS-SOA}}$ on one of the factors, a type two error, the regression analysis suggests that the dependence of $f_{\text{ROS-SOA}}$ on all parameters is significant ($p < 10^{-6}$).

Model results for SC data. The correlation between $f_{\text{ROS-SOA}}$ and the most important regressors is shown in Fig. 4. The analysis suggests that the greatest share of explained variability in $f_{\text{ROS-SOA}}$ could be attributed to $f_{44\text{-SOA}}$. An increase in $f_{44\text{-SOA}}$ by one geometric standard deviation (a factor of 1.45) resulted in our case in a doubling of the secondary PB-ROS fraction ($f_{\text{ROS-SOA}}$). This indicates that more oxygenated compounds are preferentially PB-ROS active compared to others.

The second most important parameter controlling the secondary aerosol PB-ROS content under our conditions is found to be the OH exposure. An increase in OH exposure by one geometric standard deviation (a factor of 2.7) resulted in our case in a 60 % decrease of the PB-ROS fraction in SOA ($f_{\text{ROS-SOA}}$). We note that the considerable effect size of this variable stems from its large variability, spanning a dynamic range of 2.5 orders of magnitudes (e.g. ~ 4 times more variation in OH exposure compared to $f_{44\text{-SOA}}$ would be required to achieve the same effect on $f_{\text{ROS-SOA}}$). The anti-correlation between OH exposure and $f_{\text{ROS-SOA}}$ indicates that the initially formed PB-ROS are prone to further reactions, consistent with previous observations of rapid peroxide (Krapf et al., 2016) and PB-ROS (Zhou et al., 2018) decay. The mechanism by which PB-ROS evolves remains uncertain, but may involve the oxidation of PB-ROS related molecules by OH as well as their photolysis and unimolecular decay

reaction. We note that the OH exposure increases the oxidation state of the aerosol, here represented by $f_{44\text{-SOA}}$, thereby indirectly increasing the PB-ROS content, especially in the beginning of the experiment. Therefore, the actual effect of OH exposure on $f_{\text{ROS-SOA}}$ could only be revealed when it was isolated from the $f_{44\text{-SOA}}$ effect (see Fig. 4).

The analysis suggests that $f_{43\text{-SOA}}$ and the organic mass concentrations exhibit a low, but statistically significant, effect on $f_{\text{ROS-SOA}}$ (Fig. S5). Their increase results in a decrease in the secondary PB-ROS content, consistent with the increased partitioning of moderately oxygenated components, which seem to contain less PB-ROS.

Comparison between SC and PAM chamber data. The conditions in the PAM chamber are different from those in the SC. PAM chamber experiments were conducted at high OH exposures of $\sim 10^8$ molecules cm^{-3} h, where the resulting aerosol was highly oxygenated. However, the secondary PB-ROS content of the aerosol in the PAM chamber was largely within the expected range, following consistent trends with high OH exposures and high $f_{44\text{-SOA}}$ as in the SC (Fig. 4). We examined in more detail whether the regression model parameters obtained from the SC could faithfully represent the $f_{\text{ROS-SOA}}$ measured in the PAM chamber. Indeed, the model was capable to predict, within uncertainties (2σ), the $f_{\text{ROS-SOA}}$ measured in the PAM chamber for low organic aerosol concentrations (average $21 \mu\text{g m}^{-3}$), but considerably (factor of three on average) overestimated $f_{\text{ROS-SOA}}$ at higher concentrations (average $68 \mu\text{g m}^{-3}$). This is because such a range of concentrations at high OH exposures and high $f_{44\text{-SOA}}$ was not included in the training dataset, and as a result the model slightly underestimated the effect of OA concentration on $f_{\text{ROS-SOA}}$ (e.g., a three-fold increase in OA concentration in the PAM chamber results in a decrease of $f_{\text{ROS-SOA}}$ by 45 %, while the model suggests that the same increase would only result in a 10 % decrease). Despite this, for similar conditions $f_{\text{ROS-SOA}}$ measured in the PAM chamber and the SC were similar within our uncertainties. We also note that this slight bias does not affect the main conclusions of the analysis: the secondary PB-ROS content seems to initially increase with the SOA oxidation state, which increases with OH exposure and decreases with the additional partitioning of semi-volatile components with lower secondary PB-ROS content at higher SOA concentrations, while further aging seems to result in a decay of PB-ROS.

4 Summary and Conclusions

In this study, eight wood combustion devices for log wood, pellets and wood chips, denoted as log wood boiler (LWB), log wood stove 1 (LWS1), log wood stove 2 (LWS2), log wood stove 3 (LWS3) and log wood stove 4 (LWS4), pellet boiler (PB), pellet stove (PS) and moving grate boiler (MGB), were tested. Experiments were conducted in a suite of aging tools, including the Paul Scherrer Institute mobile smog chamber (PSI-MSC, $\sim 7 \text{ m}^3$, OH exposure: $(2.6\text{-}4.8) \times 10^7$ molec cm^{-3} h), the Paul Scherrer Institute stationary smog chamber (PSI-SSC, 27 m^3 , OH exposure: $(0.13\text{-}40) \times 10^7$ molec cm^{-3} h), and the potential aerosol mass chamber (PAM chamber, OH exposure: $(11\text{-}20) \times 10^7$ molec cm^{-3} h) to investigate the particle bound reactive oxygen species (PB-ROS) formation potential of primary and aged wood combustion emissions from different combustion devices and conditions. The influence of combustion technologies, wood types (wood logs, wood pellets and wood chips), operation type (e.g. with/without ESP, automatic vs. manual operation), combustion regime (different air to fuel ratio (λ) ranging from low (λ^-), to optimum (λ^{opt}) and high values (λ^{++})), combustion phases (start, flaming, burn

out) and aging conditions (SC aging/PAM chamber aging) to PB-ROS emission factors (EF_{ROS}) were investigated. Results show that EF_{ROS} for primary and aged OA were highly variable depending on the combustion conditions and devices. For all devices and combustion conditions, EF_{ROS} substantially increased upon aging, indicating the secondary production of PB-ROS. The PB-ROS enhancement factors ranged between 4 and 20, with lower values for the MGB (~ 4) and PB under λ^{opt} combustion condition (~ 6), and higher values for the PB under λ^- and λ^{++} combustion conditions (> 10). The PB-ROS enhancement factors for all log wood stoves as well as the LWB were comparable, with an average value around 10.

The variability in the EF_{ROS} in primary and aged OA for a single device was much higher than the variability between emission factors from different devices. A part of this variability within each device could be ascribed to the combustion phase, with higher emission factors for the starting and burn out phases compared to the flaming phase. This was especially true for the aged emissions from the PS, LWS2 and LWS3. Despite this, EF_{ROS} from the PB and MGB were on average one order of magnitude lower than those from the PS, LWB and LWS1-4. This indicates that applying automatic combustion devices operated at optimum conditions, to achieve near-complete combustion, is most effective to minimize PB-ROS emissions, but also POA, SOA and BC. Although the EF_{ROS} showed somewhat different trends between devices with varying λ , a clear increase of EF_{ROS} in the aged aerosol can be observed from optimal to high lambda values; this emphasizing the important influence of the combustion conditions on EF_{ROS} . For the PB, the EF_{ROS} under λ^{opt} ($\lambda = 1.6$) did not statistically differ from that under λ^- ($\lambda \approx 1.3$) conditions for both primary and secondary emissions (Mann-Whitney, p -value = 0.43 and 0.20, respectively). When comparing the EF_{ROS} under λ^{opt} and λ^- conditions with λ^{++} ($2.7 < \lambda < 3.4$) condition, primary EF_{ROS} under λ^{opt} and λ^- conditions were on average 7 and 3 times lower than that obtained under λ^{++} condition, respectively (Mann-Whitney, p -value < 0.005 for both cases). Aged EF_{ROS} under λ^{opt} and λ^- conditions were on average 8 and 5.5 times lower than obtained under λ^{++} condition, respectively (Mann-Whitney, p -value = 0.02 for both cases). In the MGB all the burns occurred at $2.0 < \lambda < 2.2$, leading to EF_{ROS} in line with those from the PB between λ^{opt} ($\lambda = 1.6$) and λ^{++} (where λ ranged from 2.7-3.4). The combustion in all stoves (PS, LWS1-4) exhibited higher λ ($\lambda > 2.2$) due to a less controlled air supply leading to a lower combustion temperature and increased products of incomplete combustion (less efficient combustion). In this range of oxygen excess, all aged EF_{ROS} were high but without any systematic trend with λ , suggesting that also other parameters influence PB-ROS emissions. We further revealed that this variability was related to the bulk OA emissions, implying that this variation is inherent to the combustion conditions.

Nonetheless, the PB-ROS content still varied by a factor of 2.6 on average for the same OA emission factor (EF_{OA}). We used a regression model on the data of SC and PAM chamber aging experiments to identify the different parameters that control the PB-ROS secondary formation and content in OA upon aging. This regression model showed that the PB-ROS contents in SOA (represented as $f_{ROS-SOA}$) depended significantly on all the aging parameters investigated, including the fractions of m/z 44 and m/z 43 in SOA, f_{44-SOA} and f_{43-SOA} , respectively, the OH exposure and the organic aerosol mass concentration. The greatest share of explained variability in $f_{ROS-SOA}$ was attributed to f_{44-SOA} , which indicates that the more oxygenated compounds are preferentially PB-ROS active compared to others. The OH exposure was the second most important parameter controlling the aerosol PB-ROS content under our condition where the anti-correlation between OH exposure and $f_{ROS-SOA}$ indicated that initially formed PB-ROS are prone to further reactions. The organic mass and f_{43-SOA}

exhibited a low, but statistically significant effect on $f_{\text{ROS-SOA}}$. In summary, the PB-ROS content seems to increase with the SOA oxidation state, which increases with OH exposure and decreases with the additional partitioning of semi-volatile components with lower PB-ROS content at higher OA concentrations, while further aging seems to result in a decay of PB-ROS. The comparison and evolution of PB-ROS with different combustion and aging conditions in this study could eventually provide a speedy assessment of potential health risks of wood combustion emissions from different combustion and aging conditions. However, a link between PB-ROS as measured with the DCFH method and oxidative stress in cell cultures as well as health effects needs still to be established.

Data availability. Data related to this article are available online at: <https://zenodo.org/record/1200236#.WqujTk2pUkk>

Acknowledgements

This study was financially supported by the Swiss National Science Foundation (NRP 70 “Energy Turnaround”), the European Union’s Horizon 2020 research and innovation programme through the EUROCHAMP-2020 Infrastructure Activity under grant agreement No 730997, the Swiss National Science Foundation starting grant BSSGI0_155846, and the China Scholarship Council (CSC).

References

Adam, M., Schikowski, T., Carsin, A. E., Cai, Y., Jacquemin, B., Sanchez, M., Vierkötter, A., Marcon, A., Keidel, D., Sugiri, D., Al Kanani, Z., Nadif, R., Siroux, V., Hardy, R., Kuh, D., Rochat, T., Bridevaux, P.-O., Eeftens, M., Tsai, M.-Y., Villani, S., Phuleria, H. C., Birk, M., Cyrys, J., Cirach, M., de Nazelle, A., Nieuwenhuijsen, M. J., Forsberg, B., de Hoogh, K., Declerq, C., Bono, R., Piccioni, P., Quass, U., Heinrich, J., Jarvis, D., Pin, I., Beelen, R., Hoek, G., Brunekreef, B., Schindler, C., Sunyer, J., Krämer, U., Kauffmann, F., Hansell, A. L., Künzli, N., and Probst-Hensch, N.: Adult lung function and long-term air pollution exposure. ESCAPE: a multicentre cohort study and meta-analysis, *Eur. Respir. J.*, 45, 38-50, <https://doi.org/10.1183/09031936.00130014>, 2015.

Andreae, M. O., and Merlet, P.: Emission of trace gases and aerosols from biomass burning, *Global Biogeochem. Cycles*, 15, 955-966, <https://doi.org/10.1029/2000GB001382>, 2001.

Bates, J. T., Weber, R. J., Abrams, J., Verma, V., Fang, T., Klein, M., Strickland, M. J., Sarnat, S. E., Chang, H. H., Mulholland, J. A., Tolbert, P. E., and Russell, A. G.: Reactive oxygen species generation linked to sources of atmospheric particulate matter and cardiorespiratory effects, *Environ. Sci. Technol.*, 49, 13605-13612, <http://dx.doi.org/10.1021/acs.est.5b02967>, 2015.

Baltensperger, U., Dommen, J., Alfarra M. R., Duplissy J., Gaeggeler K., Metzger A., Facchini M. C., Decesari S., Finessi E., Reinnig C., Schott M., Warnke J., Hoffmann T., Klatzer B., Puxbaum H., Geiser M., Savi M., Lang D., Kalberer M., and Geiser T.: Combined determination of the chemical composition and of health effects of secondary organic aerosols: The POLYSOA Project, *J. Aerosol Med. Pulm. Drug Deliv.*, 21, 145-154, 2008.

- 555 Barmet, P., Dommen, J., DeCarlo, P. F., Tritscher, T., Praplan, A. P., Platt, S. M., Prévôt, A. S. H., Donahue, N. M., and Baltensperger, U.: OH clock determination by proton transfer reaction mass spectrometry at an environmental chamber, *Atmos. Meas. Tech.*, 5, 647-656, <http://dx.doi.org/10.5194/amt-5-647-2012>, 2012.
- 560 Beelen, R., Raaschou-Nielsen, O., Stafoggia, M., Andersen, Z. J., Weinmayr, G., Hoffmann, B., Wolf, K., Samoli, E., Fischer, P., Nieuwenhuijsen, M., Vineis, P., Xun, W. W., Katsouyanni, K., Dimakopoulou, K., Oudin, A., Forsberg, B., Modig, L., Havulinna, A. S., Lanki, T., Turunen, A., Oftedal, B., Nystad, W., Nafstad, P., De Faire, U., Pedersen, N. L., Östenson, C.-G., Fratiglioni, L., Penell, J., Korek, M., Pershagen, G., Eriksen, K. T., Overvad, K., Ellermann, T., Eeftens, M., Peeters, P. H., Meliefste, K., Wang, M., Bueno-de-Mesquita, B., Sugiri, D., Krämer, U., Heinrich, J., de Hoogh, K., Key, T., Peters, A., Hampel, R., Concin, H., Nagel, G., Ineichen, A., Schaffner, E., Probst-Hensch, N., Künzli, N., Schindler, C., Schikowski, T., Adam, M., Phuleria, H., Vilier, A., Clavel-Chapelon, F., Declercq, C., Grioni, S., Krogh, V., Tsai, M.-Y.,
- 565 Ricceri, F., Sacerdote, C., Galassi, C., Migliore, E., Ranzi, A., Cesaroni, G., Badaloni, C., Forastiere, F., Tamayo, I., Amiano, P., Dorronsoro, M., Katsoulis, M., Trichopoulou, A., Brunekreef, B., and Hoek, G.: Effects of long-term exposure to air pollution on natural-cause mortality: an analysis of 22 European cohorts within the multicentre ESCAPE project, *The Lancet*, 383, 785-795, [https://doi.org/10.1016/S0140-6736\(13\)62158-3](https://doi.org/10.1016/S0140-6736(13)62158-3), 2013.
- 570 Bølling, A. K., Totlandsdal, A. I., Sallsten, G., Braun, A., Westerholm, R., Bergvall, C., Boman, J., Dahlman, H. J., Sehlstedt, M., Cassee, F., Sandstrom, T., Schwarze, P. E., and Herseth, J. I.: Wood smoke particles from different combustion phases induce similar pro-inflammatory effects in a co-culture of monocyte and pneumocyte cell lines, *Part. Fibre Toxicol.*, 9, 45-45, <https://doi.org/10.1186/1743-8977-9-45>, 2012.
- 575 Bologa, A., Paur, H.-R., and Woletz, K.: Development and study of an electrostatic precipitator for small scale wood combustion, *Environ. Sci. & Technol.*, 5, 168-173, http://www.isesp.org/ICESP%20XII%20PAPERS/pdfs/10_wed_m/043_Bologa.pdf, 2011.
- 580 Boman, B. C., Forsberg, A. B., and Järnholm, B. G.: Adverse health effects from ambient air pollution in relation to residential wood combustion in modern society, *Scandinavian Journal of Work, Environ. & Health*, 251-260, <https://doi.org/10.5271/sjweh.729>, 2003.
- 585 Bruns, E. A., El Haddad, I., Keller, A., Klein, F., Kumar, N. K., Pieber, S. M., Corbin, J. C., Slowik, J. G., Brune, W. H., Baltensperger, U., and Prévôt, A. S. H.: Inter-comparison of laboratory smog chamber and flow reactor systems on organic aerosol yield and composition, *Atmos. Meas. Tech.*, 8, 2315-2332, <https://doi.org/10.5194/amt-8-2315-2015>, 2015.
- Bruns, E. A., El Haddad, I., Slowik, J. G., Kilic, D., Klein, F., Baltensperger, U., and Prévôt, A. S. H.: Identification of significant precursor gases of secondary organic aerosols from residential wood combustion, *Sci. Rep.*, 6, 27881, <https://doi.org/10.1038/srep27881>, 2016.
- 590 Bruns, E. A., Slowik, J. G., El Haddad, I., Kilic, D., Klein, F., Dommen, J., Temime-Roussel, B., Marchand, N., Baltensperger, U., and Prévôt, A. S. H.: Characterization of gas-phase organics using proton transfer reaction time-of-flight mass spectrometry: fresh and aged residential wood combustion emissions, *Atmos. Chem. Phys.*, 17, 705-720, <https://doi.org/10.5194/acp-17-705-2017>, 2017.
- 595 EPBE: Impact of Residential Wood Stove Replacement on Air Emissions in Canada, in, Environmental Protection Branch Environment Canada, Montréal, 2005.

Charrier, J. G., and Anastasio, C.: On dithiothreitol (DTT) as a measure of oxidative potential for ambient particles: evidence for the importance of soluble transition metals, *Atmos. Chem. Phys.*, 12, 9321-9333, 10.5194/acp-12-9321-2012, 2012.

600 Cho, A. K., Sioutas, C., Miguel, A. H., Kumagai, Y., Schmitz, D. A., Singh, M., Eiguren-Fernandez, A., and Froines, J. R.: Redox activity of airborne particulate matter at different sites in the Los Angeles Basin, *Environmental Research*, 99, 40-47, <https://doi.org/10.1016/j.envres.2005.01.003>, 2005.

605 Corsini, E., Vecchi, R., Marabini, L., Fermo, P., Becagli, S., Bernardoni, V., Caruso, D., Corbella, L., Dell'Acqua, M., Galli, C. L., Lonati, G., Ozgen, S., Papale, A., Signorini, S., Tardivo, R., Valli, G., and Marinovich, M.: The chemical composition of ultrafine particles and associated biological effects at an alpine town impacted by wood burning, *Sci Total Environ*, 587-588, 223-231, <http://dx.doi.org/10.1016/j.scitotenv.2017.02.125>, 2017.

610 Ciarelli, G., Aksoyoglu, S., El Haddad, I., Bruns, E. A., Crippa, M., Poulain, L., Äijälä, M., Carbone, S., Freney, E., O'Dowd, C., Baltensperger, U., and Prévôt, A. S. H.: Modelling winter organic aerosol at the European scale with CAMx: evaluation and source apportionment with a VBS parameterization based on novel wood burning smog chamber experiments, *Atmos. Chem. Phys.*, 17, 7653-7669, <http://dx.doi.org/10.5194/acp-17-7653-2017>, 2017.

615 DeCarlo, P. F., Kimmel, J. R., Trimborn, A., Northway, M. J., Jayne, J. T., Aiken, A. C., Gonin, M., Fuhrer, K., Horvath, T., Docherty, K. S., Worsnop, D. R., and Jimenez, J. L.: Field-Deployable, High-Resolution, Time-of-Flight Aerosol Mass Spectrometer, *Anal. Chem.*, 78, 8281-8289, <https://doi.org/10.1021/ac061249n>, 2006.

Delfino, R. J., Staimer, N., Tjoa, T., Arhami, M., Polidori, A., Gillen, D. L., George, S. C., Shafer, M. M., Schauer, J. J., and Sioutas, C.: Associations of primary and secondary organic aerosols with airway and systemic inflammation in an elderly panel cohort, *Epidemiology*, 21, 892-902, 10.1097/EDE.0b013e3181f20e6c, 2010.

620 Delfino, R. J., Staimer, N., Tjoa, T., Gillen, D. L., Schauer, J. J., and Shafer, M. M.: Airway inflammation and oxidative potential of air pollutant particles in a pediatric asthma panel, *J. Expo. Sci. Environ. Epidemiol.*, 23, 466-473, <https://doi.org/10.1038/jes.2013.25>, 2013.

625 Dockery, D. W., Pope, C. A., Xu, X., Spengler, J. D., Ware, J. H., Fay, M. E., Ferris, B. G. J., and Speizer, F. E.: An Association between Air Pollution and Mortality in Six U.S. Cities, *N. Engl. J. Med.*, 329, 1753-1759, <https://doi.org/10.1056/nejm.1993.12093292401>, 1993.

630 Drinovec, L., Močnik, G., Zotter, P., Prévôt, A. S. H., Ruckstuhl, C., Coz, E., Rupakheti, M., Sciare, J., Müller, T., Wiedensohler, A., and Hansen, A. D. A.: The "dual-spot" Aethalometer: an improved measurement of aerosol black carbon with real-time loading compensation, *Atmos. Meas. Tech.*, 8, 1965-1979, <http://dx.doi.org/10.5194/amt-8-1965-2015>, 2015.

EEA: European Union emission inventory report 1990-2011 under the UNECE Convention on Long-range Transboundary Air Pollution (LRTAP), in: EEA Technical report, EEA (European Environment Agency), Copenhagen, 2013a.

635 EEA: European Union emission inventory report 1990-2011 under the UNECE Convention on Long-range Transboundary Air Pollution (LRTAP), in: Technical report, European Environment Agency (EEA), Copenhagen, 2013b.

640 Fitzpatrick, E. M., Ross, A. B., Bates, J., Andrews, G., Jones, J. M., Phylaktou, H., Pourkashanian, M., and Williams, A.: Emission of Oxygenated Species from the Combustion of Pine Wood and its Relation to Soot Formation, *Process Saf. Environmental Protection*, 85, 430-440, <http://dx.doi.org/10.1205/psep07020>, 2007.

- 645 Fang, T., Verma, V., Bates, J. T., Abrams, J., Klein, M., Strickland, M. J., Sarnat, S. E., Chang, H. H., Mulholland, J. A., Tolbert, P. E., Russell, A. G., and Weber, R. J.: Oxidative potential of ambient water-soluble PM_{2.5} in the southeastern United States: contrasts in sources and health associations between ascorbic acid (AA) and dithiothreitol (DTT) assays, *Atmos. Chem. Phys.*, 16, 3865-3879, <http://dx.doi.org/10.5194/acp-16-3865-2016>, 2016.
- Fu, P. P., Xia, Q., Sun, X., and Yu, H.: Phototoxicity and Environmental Transformation of Polycyclic Aromatic Hydrocarbons (PAHs)—Light-Induced Reactive Oxygen Species, Lipid Peroxidation, and DNA Damage, *J. Environ. Sci. Health, Part C*, 30, 1-41, <http://dx.doi.org/10.1080/10590501.2012.653887>, 2012.
- 650 Fuller, G. W., Tremper, A. H., Baker, T. D., Yttri, K. E., and Butterfield, D.: Contribution of wood burning to PM₁₀ in London, *Atmos. Environ.*, 87, 87-94, <http://dx.doi.org/10.1016/j.atmosenv.2013.12.037>, 2014a.
- 655 Fuller, S. J., Wragg, F. P. H., Nutter, J., and Kalberer, M.: Comparison of on-line and off-line methods to quantify reactive oxygen species (ROS) in atmospheric aerosols, *Atmos. Environ.*, 92, 97-103, <http://dx.doi.org/10.1016/j.atmosenv.2014.04.006>, 2014b.
- Fullerton D. G., Semple A. S., S., Kalambo F., Malamba R., White S., Jack S., Calverley P. M., Gordon S. B.: Wood smoke exposure, poverty and impaired lung function in Malawian adults, *Int. J. Tuberc. Lung Dis.*, 15, 391-398, <http://www.ingentaconnect.com/.../ijtld>, 2011.
- 660 He, T., Yang, Z., Liu, T., Shen, Y., Fu, X., Qian, X., Zhang, Y., Wang, Y., Xu, Z., Zhu, S., Mao, C., Xu, G., and Tang, J.: Ambient air pollution and years of life lost in Ningbo, China, 6, 22485, <http://dx.doi.org/10.1038/srep22485>, 2016.
- Heringa, M. F., DeCarlo, P. F., Chirico, R., Tritscher, T., Dommen, J., Weingartner, E., Richter, R., Wehrle, G., Prévôt, A. S. H., and Baltensperger, U.: Investigations of primary and secondary particulate matter of different wood combustion appliances with a high-resolution time-of-flight aerosol mass spectrometer, *Atmos. Chem. Phys.*, 11, 5945-5957, <http://dx.doi.org/10.5194/acp-11-5945-2011>, 2011.
- 665 Huang, W., Zhang, Y., Zhang, Y., Fang, D., and Schauer, J. J.: Optimization of the Measurement of Particle-Bound Reactive Oxygen Species with 2',7'-dichlorofluorescein (DCFH), *Water Air Soil Pollut.*, 227, <http://dx.doi.org/10.1007/s11270-016-2860-9>, 2016.
- 670 Hwang, B.-F., Chen, Y.-H., Lin, Y.-T., Wu, X.-T., and Leo Lee, Y.: Relationship between exposure to fine particulates and ozone and reduced lung function in children, *Environ. Res.*, 137, 382-390, <http://dx.doi.org/10.1016/j.envres.2015.01.009>, 2015.
- 675 Liu, J. C., Wilson A., Mickley L. J., Dominici F., Ebisu K., Wang Y., Sulprizio M. P., Peng R. D., Yue X., Son J. Y., Anderson G. B., and Bell, M. L.: Wildfire-specific Fine Particulate Matter and Risk of Hospital Admissions in Urban and Rural Counties, *Epidemiology*, 28, 77-85, <http://dx.doi.org/10.1097/EDE.0000000000000556>, 2017.
- Janssen, N. A. H., Strak, M., Yang, A., Hellack, B., Kelly, F. J., Kuhlbusch, T. A. J., Harrison, R. M., Brunekreef, B., Cassee, F. R., Steenhof, M., and Hoek, G.: Associations between three specific a-cellular measures of the oxidative potential of particulate matter and markers of acute airway and nasal inflammation in healthy volunteers, *Occup. Environ. Med.*, 72, 49-56, [10.1136/oemed-2014-102303](http://dx.doi.org/10.1136/oemed-2014-102303), 2015.
- 680

- 685 Johansson, L. S., Leckner, B., Gustavsson, L., Cooper, D., Tullin, C., and Potter, A.: Emission characteristics of modern and old-type residential boilers fired with wood logs and wood pellets, *Atmos. Environ.*, 38, 4183-4195, <http://dx.doi.org/10.1016/j.atmosenv.2004.04.020>, 2004.
- 690 Johnston, F. H., Henderson, S. B., Chen, Y., Randerson, J. T., Marlier, M., Defries, R. S., Kinney, P., Bowman, D. M., and Brauer, M.: Estimated global mortality attributable to smoke from landscape fires, *Environ. Health Perspect.*, 120, 695-701, <http://dx.doi.org/10.1289/ehp.1104422>, 2012.
- Kang, E., Root, M. J., Toohey, D. W., and Brune, W. H.: Introducing the concept of Potential Aerosol Mass (PAM), *Atmos. Chem. Phys.*, 7, 5727-5744, <http://dx.doi.org/10.5194/acp-7-5727-2007>, 2007.
- 695 Kelly, F. J., and Fussell, J. C.: Size, source and chemical composition as determinants of toxicity attributable to ambient particulate matter, *Atmos. Environ.*, 60, 504-526, <http://dx.doi.org/10.1016/j.atmosenv.2012.06.039>, 2012.
- King, L. E., and Weber, R. J.: Development and testing of an online method to measure ambient fine particulate reactive oxygen species (ROS) based on the 2',7'-dichlorofluorescein (DCFH) assay, *Atmos. Meas. Tech.*, 6, 1647-1658, <http://dx.doi.org/10.5194/amt-6-1647-2013>, 2013.
- 700 Krapf, M., Kunzi, L., Allenbach, S., Bruns, E. A., Gavarini, I., El-Haddad, I., Slowik, J. G., Prevot, A. S. H., Drinovec, L., Mocnik, G., Dumbgen, L., Salathe, M., Baumlin, N., Sioutas, C., Baltensperger, U., Dommen, J., and Geiser, M.: Wood combustion particles induce adverse effects to normal and diseased airway epithelia, *Environ. Sci.-Proc. Imp.*, 19, 538-548, <http://dx.doi.org/10.1039/C6EM00586A>, 2017.
- 705 Künzi, L., Krapf, M., Daher, N., Dommen, J., Jeannet, N., Schneider, S., Platt, S., Slowik, J. G., Baumlin, N., Salathe, M., Prévôt, A. S. H., Kalberer, M., Strähle, C., Dumbgen, L., Sioutas, C., Baltensperger, U., and Geiser, M.: Toxicity of aged gasoline exhaust particles to normal and diseased airway epithelia, 5, 11801, [10.1038/srep11801](https://doi.org/10.1038/srep11801), 2015.
- 710 Lakey, P. S. J., Berkemeier, T., Tong, H., Arangio, A. M., Lucas, K., Pöschl, U., and Shiraiwa, M.: Chemical exposure-response relationship between air pollutants and reactive oxygen species in the human respiratory tract, *Sci. Rep.*, 6, 32916, <http://dx.doi.org/10.1038/srep32916>, 2016.
- 715 Landreman, A. P., Shafer, M. M., Hemming, J. C., Hannigan, M. P., and Schauer, J. J.: A macrophage-based method for the assessment of the reactive oxygen species (ROS) activity of atmospheric particulate matter (PM) and application to routine (Daily-24 h) aerosol monitoring studies, *Aerosol Sci. Technol.*, 42, 946-957, <http://dx.doi.org/10.1080/02786820802363819>, 2008.
- 720 Lee, Y. L., Wang, W.-H., Lu, C.-W., Lin, Y.-H., and Hwang, B.-F.: Effects of ambient air pollution on pulmonary function among schoolchildren, *Int. J. Hyg. and Environ. Health*, 214, 369-375, <http://dx.doi.org/10.1016/j.ijheh.2011.05.004>, 2011.
- Li, N., Sioutas, C., Cho, A., Schmitz, D., Misra, C., Sempf, J., Wang, M., Oberley, T., Froines, J., and Nel, A.: Ultrafine particulate pollutants induce oxidative stress and mitochondrial damage, *Environ. Health Perspect.*, 111, 455-460, 2003.
- 725 Li, Q., Wyatt, A., and Kamens, R. M.: Oxidant generation and toxicity enhancement of aged-diesel exhaust, *Atmospheric Environment*, 43, 1037-1042, <https://doi.org/10.1016/j.atmosenv.2008.11.018>, 2009.

Lobo, V., Patil, A., Phatak, A., and Chandra, N.: Free radicals, antioxidants and functional foods: Impact on human health, *Pharmacogn. Rev.*, 4, 118-126, <http://dx.doi.org/10.4103/0973-7847.70902>, 2010.

730 Mudway, I. S., Stenfors, N., Duggan, S. T., Roxborough, H., Zielinski, H., Marklund, S. L., Blomberg, A., Frew, A. J., Sandstrom, T., and Kelly, F. J.: An in vitro and in vivo investigation of the effects of diesel exhaust on human airway lining fluid antioxidants, *Archives of biochemistry and biophysics*, 423, 200-212, <http://dx.doi.org/10.1016/j.abb.2003.12.018>, 2004.

735 Marabini, L., Ozgen, S., Turacchi, S., Aminti, S., Arnaboldi, F., Lonati, G., Fermo, P., Corbella, L., Valli, G., Bernardoni, V., Dell'Acqua, M., Vecchi, R., Becagli, S., Caruso, D., Corrado, G. L., and Marinovich, M.: Ultrafine particles (UFPs) from domestic wood stoves: genotoxicity in human lung carcinoma A549 cells, *Mutat. Res.*, 820, 39-46, <http://dx.doi.org/10.1016/j.mrgentox.2017.06.001>, 2017.

740 Miljevic, B., Heringa, M. F., Keller, A., Meyer, N. K., Good, J., Lauber, A., DeCarlo, P. F., Fairfull-Smith, K. E., Nussbaumer, T., Burtscher, H., Prevot, A. S. H., Baltensperger, U., Bottle, S. E., and Ristovski, Z. D.: Oxidative Potential of Logwood and Pellet Burning Particles Assessed by a Novel Profluorescent Nitroxide Probe, *Environ. Sci. Technol.*, 44, 6601-6607, <http://dx.doi.org/10.1021/es100963y>, 2010.

745 Muala, A., Rankin, G., Sehlstedt, M., Unosson, J., Bosson, J. A., Behndig, A., Pourazar, J., Nyström, R., Pettersson, E., Bergvall, C., Westerholm, R., Jalava, P. I., Happonen, M. S., Uski, O., Hirvonen, M.-R., Kelly, F. J., Mudway, I. S., Blomberg, A., Boman, C., and Sandström, T.: Acute exposure to wood smoke from incomplete combustion - indications of cytotoxicity, *Part. Fibre Toxicol.*, 12, 33, <http://dx.doi.org/10.1186/s12989-015-0111-7>, 2015.

Ng, N. L., Canagaratna, M. R., Jimenez, J. L., Chhabra, P. S., Seinfeld, J. H., and Worsnop, D. R.: Changes in organic aerosol composition with aging inferred from aerosol mass spectra, *Atmos. Chem. Phys.*, 11, 6465-6474, <http://dx.doi.org/10.5194/acp-11-6465-2011>, 2011.

750 Nussbaumer T. and Kaltschmitt M.: 8.1 Begriffsdefinitionen, in M. Kaltschmitt and H. Hartmann (Eds.), *Energie aus Biomasse*: Springer, Berlin, Heidelberg, 239-247, 2000.

Nussbaumer, T.: Combustion and Co-combustion of Biomass: Fundamentals, technologies, and primary measures for emission reduction, *Energy Fuels*, 17, 1510-1521, <http://dx.doi.org/10.1021/ef030031q>, 2003.

755 Nussbaumer, T., and Lauber, A.: Formation mechanisms and physical properties of particles from wood combustion for design and operation of electrostatic precipitators, 18th European Biomass Conference and Exhibition, Lyon, ETA-Florence, 3-7 May 2010, 2010.

760 Paulsen, D., Dommen, J., Kalberer, M., Prévôt, A. S. H., Richter, R., Sax, M., Steinbacher, M., Weingartner, E., and Baltensperger, U.: Secondary Organic Aerosol Formation by Irradiation of 1,3,5-Trimethylbenzene-NO_x-H₂O in a new reaction chamber for atmospheric chemistry and physics, *Environ. Sci. Technol.*, 39, 2668-2678, <http://dx.doi.org/10.1021/es0489137>, 2005.

765 Pfaffenberger, L., Barmet, P., Slowik, J. G., Praplan, A. P., Dommen, J., Prévôt, A. S. H., and Baltensperger, U.: The link between organic aerosol mass loading and degree of oxygenation: an α -pinene photooxidation study, *Atmos. Chem. Phys.*, 13, 6493-6506, <http://dx.doi.org/10.5194/acp-13-6493-2013>, 2013.

770 Platt, S. M., El Haddad, I., Zardini, A. A., Clairotte, M., Astorga, C., Wolf, R., Slowik, J. G., Temime-Roussel, B.,
Marchand, N., Ježek, I., Drinovec, L., Močnik, G., Möhler, O., Richter, R., Barmet, P., Bianchi, F., Baltensperger, U., and
Prévôt, A. S. H.: Secondary organic aerosol formation from gasoline vehicle emissions in a new mobile environmental
reaction chamber, *Atmos. Chem. Phys.*, 13, 9141-9158, <http://dx.doi.org/10.5194/acp-13-9141-2013>, 2013.

775 Platt, S. M., Haddad, I. E., Pieber, S. M., Huang, R. J., Zardini, A. A., Clairotte, M., Suarez-Bertoa, R., Barmet, P.,
Pfaffenberger, L., Wolf, R., Slowik, J. G., Fuller, S. J., Kalberer, M., Chirico, R., Dommen, J., Astorga, C., Zimmermann,
R., Marchand, N., Hellebust, S., Temime-Roussel, B., Baltensperger, U., and Prévôt, A. S. H.: Two-stroke scooters are a
dominant source of air pollution in many cities, *Nat. Commun.*, 5, 3749, <http://dx.doi.org/10.1038/ncomms4749>, 2014.

Pope, I. C., Burnett, R. T., Thun, M. J., and et al.: Lung cancer, cardiopulmonary mortality, and long-term exposure to fine
particulate air pollution, *JAMA*, 287, 1132-1141, <http://dx.doi.org/10.1001/jama.287.9.1132>, 2002.

780 Rattanavaraha, W., Rosen, E., Zhang, H., Li, Q., Pantong, K., and Kamens, R. M.: The reactive oxidant potential of different
types of aged atmospheric particles: An outdoor chamber study, *Atmospheric Environment*, 45, 3848-3855,
<https://doi.org/10.1016/j.atmosenv.2011.04.002>, 2011.

Schmidl, C., Luisser, M., Padouvas, E., Lasselsberger, L., Rzača, M., Ramirez-Santa Cruz, C., Handler, M., Peng, G., Bauer,
H., and Puxbaum, H.: Particulate and gaseous emissions from manually and automatically fired small scale combustion
785 systems, *Atmos. Environ.*, 45, 7443-7454, <http://dx.doi.org/10.1016/j.atmosenv.2011.05.006>, 2011.

Tapanainen, M., Jalava, P. I., Mäki-Paakkanen, J., Hakulinen, P., Lamberg, H., Ruusunen, J., Tissari, J., Jokiniemi, J., and
Hirvonen, M.-R.: Efficiency of log wood combustion affects the toxicological and chemical properties of emission particles,
Inhal. Toxicol., 24, 343-355, <http://dx.doi.org/10.3109/08958378.2012.671858>, 2012.

790 Tapanainen, M., Jalava, P. I., Mäki-Paakkanen, J., Hakulinen, P., Lamberg, H., Ruusunen, J., Tissari, J., Jokiniemi, J., and
Hirvonen, M.-R.: Efficiency of log wood combustion affects the toxicological and chemical properties of emission particles,
Inhal. Toxicol., 24, 343-355, <http://dx.doi.org/10.3109/08958378.2012.671858>, 2012.

795 Tong, H., Arangio, A. M., Lakey, P. S. J., Berkemeier, T., Liu, F., Kampf, C. J., Brune, W. H., Pöschl, U., and Shiraiwa, M.:
Hydroxyl radicals from secondary organic aerosol decomposition in water, *Atmos. Chem. Phys.*, 16, 1761-1771,
<http://dx.doi.org/10.5194/acp-16-1761-2016>, 2016.

800 Tuet, W. Y., Chen, Y., Fok, S., Champion, J. A., and Ng, N. L.: Inflammatory responses to secondary organic
aerosols (SOA) generated from biogenic and anthropogenic precursors, *Atmos. Chem. Phys.*, 17, 11423-11440,
<http://dx.doi.org/10.5194/acp-17-11423-2017>, 2017.

805 U.S. Environmental Protection Administration (USEPA): National emission trends (NET) database, Emission Factor and
Inventory Group, Office of Air Quality Planning and Standards, in, Research Triangle Park, N.C., 2000.

Venkatachari, P., and Hopke, P. K.: Development and Laboratory Testing of an automated monitor for the measurement of
atmospheric particle-Bound reactive oxygen species (ROS), *Aerosol Sci. Technol.*, 42, 629-635,
<http://dx.doi.org/10.1080/02786820802227345>, 2008.

- 810 Verma, V., Ning, Z., Cho, A. K., Schauer, J. J., Shafer, M. M., and Sioutas, C.: Redox activity of urban quasi-ultrafine particles from primary and secondary sources, *Atmos. Environ.*, 43, 6360-6368, <https://doi.org/10.1016/j.atmosenv.2009.09.019>, 2009.
- Verma, V., Rico-Martinez, R., Kotra, N., King, L., Liu, J., Snell, T. W., and Weber, R. J.: Contribution of water-soluble and insoluble components and their hydrophobic/hydrophilic subfractions to the reactive oxygen species-generating potential of
815 fine ambient aerosols, *Environ. Sci. Technol.*, 46, 11384-11392, <https://doi.org/10.1021/es302484r>, 2012.
- Verma, V., Fang, T., Xu, L., Peltier, R. E., Russell, A. G., Ng, N. L., and Weber, R. J.: organic aerosols associated with the generation of reactive oxygen species (ROS) by water-soluble PM_{2.5}, *Environ. Sci. Technol.*, 49, 4646-4656, <http://dx.doi.org/10.1021/es505577w>, 2015.
- Wang, Y., Kim, H., and Paulson, S.: Hydrogen peroxide generation from α - and β -pinene and toluene secondary organic
820 aerosols, 3149-3156, 2011.
- Wang, Y., Hopke, P.K., Sun, L., Chalupa, D.C., and Utell, M.J.: Laboratory and field testing of an automated atmospheric particle-bound reactive oxygen species sampling-analysis system. *J. Toxicol.*, 419-476, <http://dx.doi.org/10.1155/2011/419476>, 2011.
- Wang, S., Sheng, Y., Feng, M., Leszczynski, J., Wang, L., Tachikawa, H., and Yu, H.: Light-induced cytotoxicity of 16
825 polycyclic aromatic hydrocarbons on the US EPA priority pollutant list in Hhuman skin HaCaT Keratinocytes: relationship between phototoxicity and excited state properties, *Environ. toxicol.*, 22, 318-327, <http://dx.doi.org/10.1002/tox.20241>, 2007.
- Ward, D. E., and Radke, L. F.: Emission measurements from vegetation fires: A comparative evaluation of methods and
830 results, in: *Fire in the Environment: The Ecological, atmospheric and Climatic Importance of Vegetation Fires*, edited by: Crutzen, P. J., and Goldammer, J. G., John Wilry, Chichester UK, 53-56, 1993.
- Weber, S., Gaëlle, U., Calas, A., Chevrier, F., Besombes, J. L., Charron, A., Salameh, D., Ježek, I., Močnik, G., and Jaffrezo, J. L.: An apportionment method for the Oxydative Potential to the atmospheric PM sources: application to a one-year study
835 in Chamonix, France, *Atmos. Chem. Phys. Discuss.*, 2018, 1-19, <https://doi.org/10.5194/acp-2017-1053>, 2018.
- Yap, S. G. P.: The Potential Impact of Residential Wood Burning Regulations in a California Region: Concurrent Wintertime Reductions in Ambient Pollution and Cardiovascular Mortality, ISEE 20th Annual Conference, Pasadena, California, USA, 2008.
- 840 Zhang, X., Hecobian, A., Zheng, M., Frank, N. H., and Weber, R. J.: Biomass burning impact on PM_{2.5} over the southeastern US during 2007: integrating chemically speciated FRM filter measurements, MODIS fire counts and PMF analysis, *Atmos. Chem. Phys.*, 10, 6839-6853, <http://dx.doi.org/10.5194/acp-10-6839-2010>, 2010.
- Zhang, X., Staimer, N., Tjoa, T., Gillen, D. L., Schauer, J. J., Shafer, M. M., Hasheminassab, S., Pakbin, P., Longhurst, J.,
845 Sioutas, C., and Delfino, R. J.: Associations between microvascular function and short-term exposure to traffic-related air pollution and particulate matter oxidative potential, *Environmental health : a global access science source*, 15, 81, <http://dx.doi.org/10.1186/s12940-016-0157-5>, 2016.

850 Zhou, J., Bruns, E. A., Zotter, P., Stefenelli, G., Prévôt, A. S. H., Baltensperger, U., El-Haddad, I., and Dommen, J.:
Development, characterization and first deployment of an improved online reactive oxygen species analyzer, *Atmos. Meas.*
Tech., 11, 65-80, <http://dx.doi.org/10.5194/amt-11-65-2018>, 2018.

Zhou, M., Diwu, Z., Panchuk-Voloshina, N., and Haugland, R. P.: A stable nonfluorescent derivative of resorufin for the
fluorometric determination of trace hydrogen peroxide: applications in detecting the activity of phagocyte NADPH oxidase
and other oxidases, *Anal. biochem.*, 253, 162-168, <http://dx.doi.org/10.1006/abio.1997.2391>, 1997.

855

860

865

870

Table 1. Overview of combustion devices and test aspects.

Aging conditions	Combustion devices	Test aspects
PAM chamber ($T = \sim 38\text{ }^{\circ}\text{C}$, RH = 20 – 25 %)	Pellet boiler (PB)	EF _{ROS} of different burning regimes [#] (λ^{++} , λ^{-} , λ^{opt})
	Moving grate boiler (MGB)	EF _{ROS} of full/part load; With/without electrostatic precipitator (ESP)
	Pellet stove (PS)	EF _{ROS} of different burning phases**
	Log wood boiler (LWB)	EF _{ROS} of different burning phases**
	Log wood stove 1 (LWS1)	EF _{ROS} of different burning phases**
	Log wood stove 2 (LWS2)	EF _{ROS} of different burning phases**
	Log wood stove 3 (LWS3)	EF _{ROS} of different burning phases** Secondary ROS formation
PSI-MSD ($\sim 7\text{ m}^3$) $T = -10\text{ or }15^{\circ}\text{C}$, RH = 50 %	Log wood stove 4 (LWS4)	Flaming phase, aging temperature; Secondary ROS formation
PSI-SSC ($\sim 27\text{ m}^3$) Ambient T (22.5 $^{\circ}\text{C}$), RH = 50 %	Log wood stove 4 (LWS4)	Flaming phase Secondary ROS formation

^{#, **} The definitions of the burning regimes and burning phases are described in sect. 2.2.

Table 2. Characterization of primary emissions from PAM chamber and SC aging experiments*

Devices	Test aspects		Number of tests	MCE	λ	PB-ROS nmol kg ⁻¹	Total PM mg kg ⁻¹	Org mg kg ⁻¹	OM: OC	O:C	H:C
PB	λ^-		3	[0.991 0.992]	[1.29 1.30]	[345 882]	[246 301]	[56 62]	[2.1 2.4]	[0.7 0.9]	[1.3 1.4]
	λ^{opt}		7	[0.999 0.999]	[1.59 1.64]	[288 2325]	[50 69]	[22 29]	[2.7 2.8]	[1.1 1.2]	[1.3 1.4]
	λ^{++}		15	[0.963 0.983]	[3.02 3.11]	[1940 5944]	[33 61]	[15 26]	[2.5 2.6]	[0.9 1.0]	[0.9 1.0]
MGB	Full load	Before ESP	5	[0.999 0.999]	[1.99 2.04]	[1758 2034]	[65 100]	[27 48]	[3.1 3.1]	[1.4 1.4]	[1.1 1.3]
		After ESP	3	[0.999 0.999]	[3.91 3.99]	[775 1098]	[3 4]	[1 2]	[2.3 2.7]	[0.7 1.0]	[1.2 1.4]
	Part load	Before ESP	6	[0.999 0.999]	[2.12 2.30]	[780 4083]	[19 25]	[8 9]	[2.1 2.3]	[0.6 0.8]	[1.1 1.3]
PS	All burning phases		5	[0.989 0.995]	[4.97 7.59]	[5376 36415]	[204 625]	[60 427]	[2.2 2.5]	[0.8 1.0]	[1.1 1.3]
LWB			20	[0.904 0.999]	[1.47 2.49]	[4307 27590]	[262 741]	[111 277]	[2.5 2.9]	[1.0 1.4]	[1.1 1.2]
LWS1			6	[0.850 0.933]	[3.57 7.05]	[5915 52528]	[381 572]	[142 379]	[2.3 2.4]	[0.9 1.0]	[1.2 1.2]
LWS2			6	[0.948 0.976]	[3.51 4.31]	[141457 249755]	[49 98]	[49 98]	[2.3 2.4]	[0.9 1.0]	[1.2 1.3]
LWS3			19	[0.930 0.968]	[4.61 9.57]	[12160 61258]	[151 356]	[14 55]	[1.9 2.1]	[0.5 0.6]	[1.4 1.6]
LWS4	Flaming		5	[0.972 0.975]	[3.0 3.6]	[37766 57403]	[171 440]	[83 162]	[1.6 1.7]	[0.30 0.45]	[1.3 1.5]

* Values of each parameter are described as [a, b], where a and b represent the 25th and 75th percentile of the averages from several experiments and the data points considered for the calculations were restricted to the time period of the PB-ROS measurements